

特约专栏

# First-Principles Thermodynamics at Finite Temperatures: Perspective on Ordered and Disordered Phases

Shunli SHANG, Yi WANG, Zi-kui LIU

(Department of Materials Science and Engineering, The Pennsylvania State University,  
University Park, Pennsylvania 16802, USA)

**Abstract:** A longstanding issue of first-principles calculations is to predict thermodynamic properties for a disordered phase at finite temperatures. Here, we show that a recent advance for this issue is the partition function approach in terms of microstates, which is the key for both ordered phase with one primary microstate and disordered phase consisting of two and more noticeable microstates. For a given microstate, first-principles phonon calculations in terms of the quasiharmonic approach provide a practical pathway to predict its thermodynamic properties. In the present paper, a summary of properties predicted at finite temperatures is presented, and examples are given for ordered phases of anti-fluorite  $\text{Li}_2\text{S}$ , hcp Mg, and fcc Ni as well as disordered phases of  $\text{Cu}_2\text{ZnSnS}_4$  (CZTS) and fcc Ce. It is shown that (i) the extension from “phase” to “microstate” opens an avenue to quantitatively tailor anomalous properties such as phase transition and thermal expansion anomaly, and these anomalies are traceable from the microstate configurational entropy, and (ii) these microstates can be considered as the building blocks, i. e., the genome, of materials.

**Key words:** first-principles phonon calculations; quasiharmonic approach; microstate; ordered phase; disordered phase; thermodynamic properties

CLC number: TG111 Document code: A Article ID: 1674-3962(2015)04-0297-08

## 有限温度第一原理热力学：关于处理 有序相和无序相的观点

商顺利, 王 义, 刘梓葵

(宾夕法尼亚州立大学材料科学与工程系, 美国 宾夕法尼亚州大学城, PA 16802)

**摘 要:** 第一原理计算一个悬而未决的难题是预测无序相在有限温度下的热力学性能。作者团队指出该难题的最新解决思路是采用可以处理微观组态的配分函数方法, 该方法已成为处理只有一种主要微观组态构成的有序相以及有多种明显的微观组态构成的无序相的关键。结合第一原理声子计算和准简谐近似可以有效地预测任意一个给定微观组态的热力学性质。总结了作者团队在第一原理热力学方面的最新研究进展并具体给出了有序相方面的例子:  $\text{Li}_2\text{S}$ , hcp Mg 和 fcc Ni, 以及无序相方面的例子:  $\text{Cu}_2\text{ZnSnS}_4$  (CZTS) 和 fcc Ce。同时指出: ①从常用的“相”扩展到“微观组态”开辟了一条定量研究材料相变、热膨胀等异常性能的新途径, 而这些异常性能的起源可以追溯到“微观组态构型熵”; ②这些微观组态也可以认为是材料基因组的基本组成模块。

**关键词:** 第一原理声子计算; 准简谐近似; 微观组态; 有序相; 无序相; 热力学性质

### 1 Introduction

Great success has been made in recent years in first-principles thermodynamics of ordered phases with the input being atomic numbers and crystal structures<sup>[1]</sup>. Furthermore with the quasiharmonic approach<sup>[2-3]</sup>, the density functional theory (DFT) based first-principles calculations yield quantitative Helmholtz energy as a function of volume and temperature for a given structure, i. e., the ordered phase. However, the treat-

ment of disordered phase due to uncertainty of atomic occupations still remains one of the longstanding issues within the first-principles community<sup>[4]</sup>. After years of efforts, two approaches are widely used for substitutionally disordered phases<sup>[4]</sup>: the cluster expansion method (CEM)<sup>[5-7]</sup> and the special quasirandom structure (SQS)<sup>[8-9]</sup>. In CEM, first-principles energetics of a variety of structures (microstates) with each possessing a specified configuration is mapped onto a generalized Ising-like Hamiltonian to determine the effective cluster interactions (ECI's), and then, the lowest energy configurations as well as energies for disordered configurations can be predicted for various concentrations according to the ECI's. An SQS represents a fully random alloy by means of a special configuration with a few (4~32) atoms to mimic the most relevant pair and multisite correlation functions of the solution<sup>[8-9]</sup>. SQS can be

Received date: 2014-12-22

Corresponding author: Shunli Shang, Senior Research Associate,  
Email: sus26@psu.edu

DOI: 10.7502/j.issn.1674-3962.2015.04.06

considered as a mixture of various microstates, i. e., an average structure for a given lattice. Hence, energy (also true for other properties) of SQS should be in the middle of the energy landscape of all microstates<sup>[10–11]</sup>. It is worth mentioning that the truncated error in determining ECI's is unavoidable, making the CEM predicted low energy configurations less accurate<sup>[12]</sup>. In CEM, other approaches such as Monte Carlo<sup>[6]</sup> and the cluster variation method<sup>[13]</sup> need to be used to describe free energy at finite temperatures. SQS is only a special microstate, which cannot predict the expected low energy of disordered phase and handle its configurational entropy at finite temperatures. The shortcomings of SQS and CEM imply that new approaches for disordered phase are expected.

Recently we show that a macroscopically homogeneous single phase can be depicted as a statistical ensemble consisting of unique microstates with each possessing a distinguishable atomic, polar, magnetic, or other configuration<sup>[10, 14]</sup>. Consequently, an ordered phase is an ensemble dominated by one primary microstate, while a disordered phase possesses two and more types of noticeable microstates. The extension from the commonly used “phase” to a statistical ensemble of “microstates” is more or less a natural extension of the aforementioned CEM and SQS, and furthermore, the concept of the fluctuation of microstates opens an avenue to quantitatively tailor various macroscopic phenomena such as phase transition, Curie temperature, and anomalies of thermal expansion and heat capacity<sup>[10, 14]</sup>, see details in Sections 2 and 3.

Understanding materials properties from microstates is also in line with the principle of statistic mechanics<sup>[15]</sup>: The microstates give more detailed information about the system, since the information needed to define a microstate is enough to allow one to calculate the corresponding macroscopic state but not vice versa. In addition, these microstates can be considered as the building blocks, i. e. the genome, of materials on the basis of the authors' perspective<sup>[16]</sup>. In analogy to the genome concept in biologic systems, the “mutation” of materials genome can thus be viewed as the manifestation of statistic probability of various microstates. These “mutations” provide a theoretic foundation to understand materials properties, especially various anomalies such as colossally positive, zero, or negative thermal expansion, gigantic electrocaloric and electromechanical responses, anomalously low thermal conductivity, and spin distributions<sup>[10, 14, 16]</sup>. It is noted that each microstate possesses “normal” behaviors, while “anomalous” behaviors originate from the fluctuation of microstates, i. e., the microstate configurational entropy<sup>[14]</sup>, see details in Section 2. Properties of interest for each microstate are therefore the foundation for the present partition function model. Relevant to thermodynamic properties at finite temperatures, the key is to determine phonon properties for each microstate. To this end, a parameter-free mixed-space approach<sup>[17]</sup>, as implemented in the YPHON code<sup>[18]</sup>, can be employed, which makes full use of the accurate force constants from the real-space supercell approach and the dipole-dipole interactions from the linear response theory in the reciprocal space. For polar materials, the mixed-space ap-

proach can adequately account for the long range dipole-dipole interactions which lead to the well-known LO-TO (longitudinal optical and transverse optical) splitting.

The present work aims to provide a perspective on the current advance of first-principles thermodynamics for both ordered and disordered phases. To this vision, the partition function approach in terms of a statistical ensemble of microstates is presented firstly in Section 2 for methodology. For each microstate, i. e., the ordered phase, the quasiharmonic approach to determine its thermodynamic properties is briefly discussed, where the vibrational contribution is accounted for using the YPHON code<sup>[17–18]</sup> for both polar and nonpolar materials (microstates). In the Section 3 for results, examples are given for ordered phases of anti-fluorite  $\text{Li}_2\text{S}$ , hcp Mg, and fcc Ni as well as disordered phases of  $\text{Cu}_2\text{ZnSnS}_4$  (CZTS) and fcc Ce. The associated anomalous properties for disordered phases are also presented and discussed in light of the fluctuation of microstates, i. e., the microstate configurational entropy.

## 2 Methodology

Our perspective on first-principles thermodynamics is detailed here for both ordered and disordered phases, including the partition function approach in terms of microstates, the quasiharmonic approach for each microstate by means of phonon calculations, and the quasistatic approach for properties of interest at finite temperatures.

### 2.1 Partition function approach in terms of microstates

As aforementioned, we recently went one step further than the commonly used “phase” to understand the origin as well as to quantitatively predict anomalous properties in nature. We propose that a macroscopically homogeneous single phase is a statistical ensemble composed of a number of unique “microstates” with each possessing a given atomic, polar, magnetic, or other configuration<sup>[10, 14, 19–22]</sup>. In terms of the conventional phase stability, the microstate with the lowest free energy is the stable state, and all others with higher free energies are metastable states<sup>[10, 14]</sup>. We postulate this competing system (single phase) belongs to a canonical ensemble under the  $NVT$  framework or a grand canonical ensemble under the  $\mu VT$  framework, where  $N$  is the number of particles,  $V$  is the volume,  $T$  is the temperature, and  $\mu$  is the chemical potential. For example of a  $NVT$  ensemble, the canonical partition function is,

$$Z = \sum_{\sigma} Z^{\sigma} = \sum_{\sigma} w^{\sigma} \exp(-\beta F^{\sigma}) \quad (1)$$

where  $Z^{\sigma}$  represents the partition function of the individually distinguishable microstate  $\sigma$ ,  $w^{\sigma}$  is the degeneracy factor (multiplicity) of  $\sigma$ ,  $\beta = 1/(k_B T)$  with  $k_B$  the Boltzmann constant, and  $F^{\sigma}$  is the Helmholtz energy of  $\sigma$  as a function of  $V$  and  $T$ . The total Helmholtz energy of the  $NVT$  ensemble is<sup>[14, 23–24]</sup>,

$$F = -\ln(Z)/\beta = \left( \sum_{\sigma} x^{\sigma} F^{\sigma} \right) - TS_{MCE} \quad (2)$$

where  $x^{\sigma} = Z^{\sigma}/Z$  is the thermal probability of microstate  $\sigma$  with the  $w^{\sigma}$  included. Note that the value of  $x^{\sigma}$  within a given ensemble is not random, but according to the free energy of  $\sigma$ .  $S_{MCE}$  is the microstate configurational entropy introduced automatically

due to the competing stable and metastable microstates,

$$S_{MCE} = -k_B \sum_{\sigma} x^{\sigma} \ln(x^{\sigma}/w^{\sigma}) \quad (3)$$

It is worth mentioning that the entropy term  $-TS_{MCE}$  in Eq. (2) reduces the free energy  $F$  due to  $x^{\sigma} \leq 1$  and  $w^{\sigma} \geq 1$ , making the competing  $NVT$  system more stable at high temperatures than any single microstate. Consequently, the total entropy of the system equals to  $(\sum_{\sigma} x^{\sigma} S^{\sigma}) + S_{MCE}$ , where the first term is a linear combination of entropies of all microstates, and the second term  $S_{MCE}$  stems from the fluctuation of microstates and affects the properties of the homogeneous single phase dramatically, resulting in non-linear behaviors beyond the linear combination in the first term. Examples can be found in our previous works, such as the critical temperature of phase transition and anomalous thermal expansion in  $\text{Cu}_2\text{ZnSnS}_4$  (CZTS) [10], Curie temperatures and anomalous heat capacities in bcc Fe [19] and fcc Ni [25], negative thermal expansion in Invar alloy  $\text{Fe}_3\text{Pt}$  [20], colossally positive thermal expansion in fcc Ce [21, 24], and magnetic excitation in  $\text{BeFe}_2\text{As}_2$  [22].

## 2.2 Quasiharmonic approach for each microstate

As shown in Eqs. (1) and (2), the key to determine the total Helmholtz energy is the Helmholtz energy of each microstate  $\sigma$ , i. e., the  $F^{\sigma}$ . Based on the quasiharmonic approach,  $F^{\sigma}$  is usually represented by [2-3],

$$F^{\sigma}(V, T) = E^{\sigma}(V) + F_{vib}^{\sigma}(V, T) + F_{el}^{\sigma}(V, T) \quad (4)$$

where  $E^{\sigma}(V)$  is the static energy at 0 K without the zero-point vibrational energy, determined by fitting the first-principles energy versus volume data points according to for example a four-parameter Birch-Murnaghan equation of state (EOS) [2],

$$E^{\sigma}(V) = a + bV^{-2/3} + cV^{-4/3} + dV^{-2} \quad (5)$$

where  $a$ ,  $b$ ,  $c$ , and  $d$  are fitting parameters. Equilibrium properties resulted from this EOS include volume ( $V_0$ ), energy ( $E_0$ ), bulk modulus ( $B_0$ ) and its pressure derivative ( $B'_0$ ) [2]. The second term,  $F_{vib}^{\sigma}(V, T)$ , and the third term,  $F_{el}^{\sigma}(V, T)$ , are related to contributions at finite temperatures. The key is to find the number of configurations, i. e., the phonon density of state (DOS) and the electronic DOS [2-3]. In practice,  $F_{vib}^{\sigma}$  can be predicted from the Debye model for the sake of simplicity or first-principles phonon calculations for accurate results [2]. Regarding phonon calculations, the aforementioned mixed-space approach [17], as implemented in the YPHON code [18], can be applied for both polar and nonpolar materials. Using this mixed-space approach, lots of phonon properties have been investigated for such as the polar crystals of Li-ion battery materials  $\text{LiMPO}_4$  ( $M = \text{Mn, Fe, Co, and Ni}$ ) [26] and  $\text{Li}_2\text{CO}_3$  [27], solar cell materials CZTS [10], energy-related  $\text{TiO}_2$  [28], Mott-Hubbard insulators  $\text{Cr}_2\text{O}_3$  [29], NiO and MnO [30], photocatalyst  $\text{SrTiO}_3$  [31], multiferroic  $\text{BiFeO}_3$  [32], superconductivity  $\text{Sr}_2\text{RuO}_4$  [33], and fluorite compounds  $\text{CaF}_2$  and  $\text{CeO}_2$  [34].

## 2.3 Quasistatic approach for temperature-dependent properties

For properties that are mainly controlled by volume change with the increase of temperature, a quasistatic approach [35-36] can be used to predict the temperature-dependent properties in terms of the property-volume relationship from

first-principles directly and the volume-temperature relationship from the quasiharmonic approach of Eq. (4). According to this approach, elastic properties and direction-dependent thermal expansion coefficients have been predicted at finite temperatures for e. g.  $\text{Al}_{12}\text{Mg}_{17}$  [37],  $\text{Mg}_2X$  ( $X = \text{Si, Ge, Sn, and Pb}$ ) [38], Mg-La compounds [39],  $\text{Al}_2\text{O}_3$  [35], Ni-based superalloys [40], fcc-based metal nitrides [41], and cellulose [42]. Besides elasticity and thermal expansion, ideal shear strength and stacking fault energy were also predicted for fcc Ni at finite temperatures [43].

## 3 Selected results and discussion

Five examples are shown in this Section to demonstrate the current advance of first-principles thermodynamics (see Sections 1 and 2) for both ordered phases (anti-fluorite  $\text{Li}_2\text{S}$ , hcp Mg, and fcc Ni) and disordered phases (CZTS and fcc Ce). Since ordered phase can be depicted by one primary microstate, the normal first-principles calculations can be used. For disordered phase with two and more noticeable microstates, the partition function approach will be employed.

### 3.1 Ordered phase containing one major microstate

The first example is a polar crystal  $\text{Li}_2\text{S}$  with anti-fluorite structure (space group  $Fm\bar{3}m$ ). All DFT-based first-principles calculations of  $\text{Li}_2\text{S}$  were performed using the VASP code [44] together with the ion-electron interaction described by the projector augmented wave method [45]. Several exchange-correlation (X-C) functionals and methods were employed based on our tests for sulfur and sulfur-containing materials [46], including the generalized gradient approximation (GGA) by Perdew-Burke-Ernzerhof (PBE) [47], the PBE improved for densely packed solids and their surfaces (PBEsol) [48], the semi-empirical van der Waals correction (the D3 method) [49], and a hybrid X-C functional of HSE06 [50] (25% Hartree-Fock exchange plus 75% PBE or PBE + D3). During VASP calculations, a 360 eV plane wave energy cutoff was employed and a k-point mesh of  $16 \times 16 \times 16$  was used for the 12-atom crystallographic cell (or the 3-atom primitive cell for time-consuming HSE06 calculations). The reciprocal-space energy integration was performed by the tetrahedron method incorporating a Blöchl correction [51]. The self-consistency of total energy was converged to at least  $10^{-6}$  eV/atom. Phonon calculations were performed by the YPHON code [18] in terms of a 96-atom  $2 \times 2 \times 2$  supercell together with the  $4 \times 4 \times 4$  k-point mesh. Other details of first-principles and phonon calculations can be found in the literature [10, 26-34].

Table 1 summarizes the results of  $\text{Li}_2\text{S}$  from first-principles calculations, including structural properties (equilibrium volume  $V_0$ , bulk modulus  $B_0$  and its pressure derivative in terms of Eq. (5)), enthalpy of formation ( $\Delta H$  with the references states of  $\alpha$ -S and bcc Li), band gap, and phonon frequencies at the  $\Gamma$  point. Available measurements [52-55] are also shown for comparison. It is found that the best X-C functional is PBEsol (and HSE06 with PBE) for  $V_0$  predictions. Note that the zero-point vibrational energy will increase the predicted  $V_0$  but it was ignored. The van der Waals correction (using the D3 method)

gives a better prediction for both  $B_0$  and  $\Delta H$ . As for  $B'_0$ , it is a sensitive value and the measured value of  $(2.1 \pm 0.4)$  [54] is for reference only due to the scattered experimental data points. We point out that around 4 is expected for  $\text{Li}_2\text{S}$  based on first-principles calculations. Regarding band gap, no experimental data are available for  $\text{Li}_2\text{S}$ . The present value from HSE06 is around 4.3 eV and the EV-GGA method predicted a value of 4.55 eV [56]. According to the general practice of first-principles calculations, a reliable band gap can be predicted from HSE06 or EV-GGA. Therefore,  $\text{Li}_2\text{S}$  is a wide gap semiconductor with an indirect band gap around 4.4 eV. At the  $\Gamma$  point

of  $\text{Li}_2\text{S}$ , computed values of the  $T_{2g}$  Raman mode agree with experimental data [55], in particular for the predictions from PBE and PBEsol. Regarding the  $T_{1u}$  infrared mode, a large LO-TO splitting is predicted with the LO frequency 30% and above higher than the TO frequency. As an example, Figure 1 illustrates the phonon dispersions of  $\text{Li}_2\text{S}$ , showing a large LO-TO splitting at the  $\Gamma$  point and a good agreement between experiments and calculations (by PBEsol). At finite temperatures, computed entropy and heat capacity at constant pressure ( $p = 0$  GPa) from the quasi-harmonic approach agree reasonably well with the SGTE data [52], see Figure 2. In addition, the van der

Table 1 Calculated and experimental properties for anti-fluorite  $\text{Li}_2\text{S}$  with space group , including the enthalpy of formation ( $\Delta H$ , the reference states are-S and bcc Li [46], and the unit is kJ/mol-atom), the equilibrium volume ( $V_0$ ,  $\text{\AA}^3/\text{atom}$ ), bulk modulus ( $B_0$ , GPa) and its pressure derivative ( $B'_0$ ), the band gap (BG, eV), and the Raman (R) and infrared (IR) phonon frequencies at the point ( $T_{2g}$  and  $T_{1u}$  modes with the unit of  $\text{cm}^{-1}$ , and both the TO and LO modes are also shown for  $T_{1u}$ )

Methods	$\Delta H$	$V_0$	$B_0$	$B'_0$	BG	$T_{2g}$ (R)	$T_{1u}$ (IR) (TO/LO)
PBE	-129.6	15.619	40.6	4.06	3.35	379	328/455
PBE + D3	-137.1	14.777	46.2	4.24	3.33	404	359/478
PBEsol	-129.6	15.188	41.6	4.28	3.16	384	337/459
PBEsol + D3	-135.1	14.567	46.1	3.97	3.14	411	364/479
HSE06 (PBE)		15.340	43.2	4.07	4.32		
HSE06 (PBE + D3)		14.559	48.8	4.10	4.28		
Expt.	-148.8 <sup>a</sup>	15.34 <sup>b</sup>	45.7 $\pm$ 2.7 <sup>c</sup>	2.1 $\pm$ 0.4 <sup>d</sup>	N/A <sup>e</sup>	380 <sup>f</sup>	

Note: a SGTE (SSUB) data at 298 K estimated based on experimental results [52], b measured lattice parameter  $a = 5.689$   $\text{\AA}$  at 10 K [53], c based on  $c_{11} = 95.4 \pm 3.5$  and  $c_{12} = 20.9 \pm 2.3$  GPa via the measured acoustic phonons at 15 K [53], d fitted results based on measured data at high pressures for reference only [54], e experimental data not available, other predictions of indirect band gap from 3.14 to 4.55 eV [56], f measured at 18 K [55]

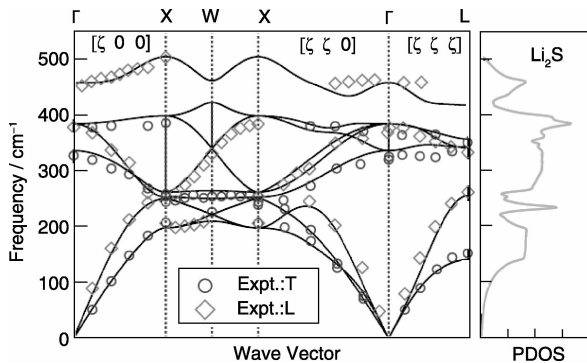


Fig. 1 Calculated phonon dispersions and phonon density of state (PDOS) of anti-fluorite  $\text{Li}_2\text{S}$  at its theoretical equilibrium volume in terms of PBEsol (see Table 1). Measured dispersions at 15 K by neutron scattering are also shown for comparison, including both the longitudinal (L) and transverse (T) polarizations [53]

Waals correction using the D3 method gives a better description of thermodynamic properties, agreeing with our previous findings for sulfur and sulfur-containing materials [46]. The example of  $\text{Li}_2\text{S}$  indicates that (i) structural properties as well as electronic structures (e.g. band gap) can be predicted well in terms of a selected X-C functional, and (ii) phonon and associated thermodynamics can be predicted well using the YPHON code.

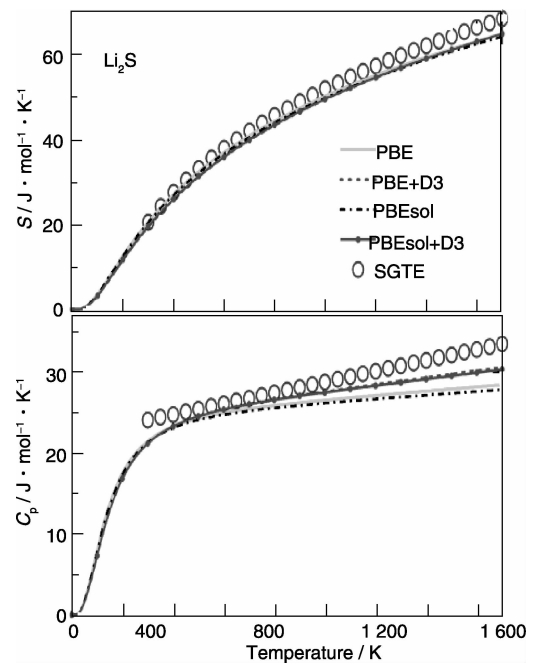


Fig. 2 Calculated entropy ( $S$ ) and heat capacity at constant pressure ( $C_p$ ,  $p = 0$  GPa) for anti-fluorite  $\text{Li}_2\text{S}$  in terms of the quasi-harmonic phonon approach and different X-C functionals. SGTE (SSUB) data are also shown for comparison [52]

The second example is Mg with hcp structure. Figure 3 shows the direction-dependent linear thermal expansion coefficients and the isothermal and isentropic elastic constants  $c_{ij}$ 's of hcp Mg<sup>[57]</sup>. These results were predicted based on the aforementioned quasistatic approach (see Section 2.3) and agree reasonably well experimental data<sup>[57]</sup>. Also based on the quasistatic approach, Figure 4 shows the third example: computed ideal shear strength of fcc Ni under both the pure alias and the pure affine shear deformations (see details in[43]). These two examples (hcp Mg and fcc Ni) indicate that the quasistatic approach is an effective but simple approach to predict properties at finite temperatures.

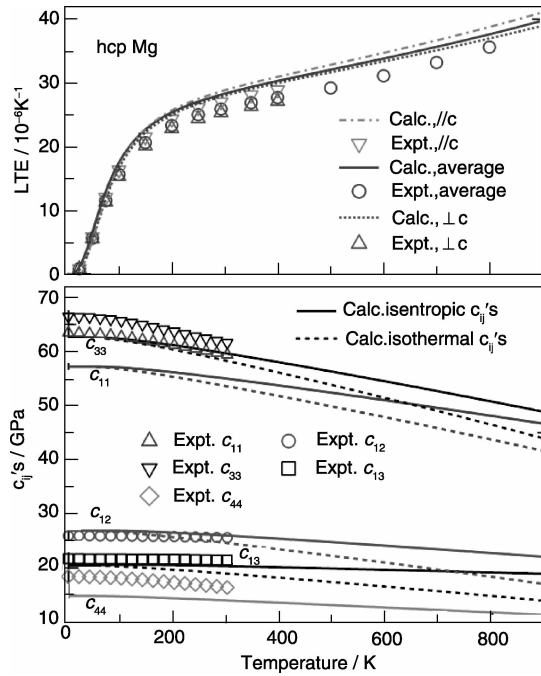


Fig. 3 Predicted linear thermal expansion coefficients (LTE) along the a- and c-axis directions of hcp Mg and the isentropic and isothermal elastic constants  $c_{ij}$ 's of hcp Mg in terms of the quasistatic approach. Details of first-principles methodology and references for experimental data (the symbols) are given in the literature [57]

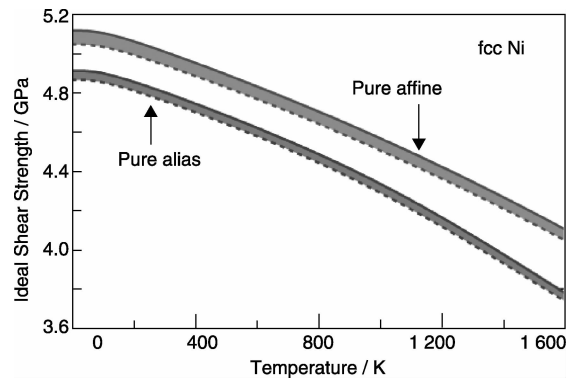


Fig. 4 Predicted ideal shear strength of fcc Ni in terms of the quasistatic approach. Details of first-principles methodology and shear schemes (pure affine and pure alias shear deformations) are given in the literature [43]

For ordered phase with one major microstate, the examples of  $\text{Li}_2\text{S}$ , hcp Mg, and fcc Ni as well as the ones mentioned in Section 2 indicate that first-principles is emerging as a routine technique to predict properties at finite temperatures in terms of a selected X-C functional and a proper methodology, for example the mixing-space approach, the quasiharmonic approach, and/or the quasistatic approach.

### 3.2 Disordered phase containing more microstates

For disordered phase containing two and more microstates, the first example is  $\text{Cu}_2\text{ZnSnS}_4$  (CZTS). It was found that cation disorder plays a major role in the performance deterioration of CZTS-based photovoltaic materials, in particular the Cu/Zn disorder occurs on Wyckoff sites 2c and 2d of the ground-state kesterite (KS) structure with space group  $\bar{1}4$  (#82)<sup>[10]</sup>. To probe the effect of Cu/Zn disorder, a 64-atom supercell was built by considering the distributions of Cu and Zn within the 2c and 2d sites, resulting in 255 independent microstates among a total of  $C_{16}^8 = 12\,870$  microstates<sup>[10]</sup>. The canonical partition function under the NVT framework was used together with the Helmholtz energies for the key low energy microstates predicted by the quasiharmonic phonon approach. Since the non-linear behaviors are regulated by the microstate configurational entropy,  $S_{\text{MCE}}$ , see Eqs. (2) and (3), Figure 5 shows the variation of  $S_{\text{MCE}}$  for CZTS as a function of temperature as well as the corresponding heat capacity at constant pressure ( $C_p$ ) and linear thermal expansion coefficient (TEC) resulted from  $S_{\text{MCE}}$ <sup>[10]</sup>. Similar to the magnetic phases such as bcc Fe<sup>[19]</sup>, fcc Ni<sup>[25]</sup>,  $\text{Fe}_3\text{Pt}$ <sup>[20]</sup>, and fcc Ce<sup>[21, 24]</sup>, the second-order phase transition of CZTS can be judged by the maximum of  $C_p$  or TEC. Figure 5 indicates that the estimated phase transition temperature is 490 K from  $C_p$  (based on  $S_{\text{MCE}}$  only) or 470 K from the linear TEC (based on  $S_{\text{MCE}}$  only). These critical temperatures (470 and 490 K) agree satisfactorily with the measured critical temperature ( $533 \pm 10$  K) using the near-resonant Raman scattering<sup>[58]</sup> and the anomalous increase of thermal expansion observed around 513 K<sup>[59]</sup>. Note that more details and tests using different supercells can be found in [10].

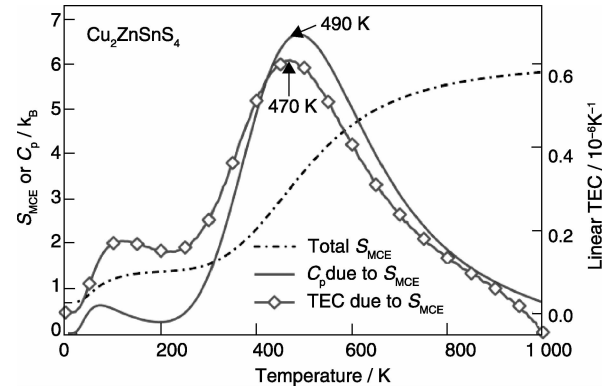


Fig. 5 Calculated total microstate configurational entropy  $S_{\text{MCE}}$  and associated heat capacity at constant pressure ( $C_p$ ,  $p = 0$  GPa) and linear thermal expansion coefficients (TEC) in terms of the 64-atom supercell of  $\text{Cu}_2\text{ZnSnS}_4$  (CZTS). Details of first-principles methodology can be found in the literature [10]

The second example is a magnetic element fcc Ce, which possesses a colossal positive thermal expansion (CPTE) due to phase transition from the nonmagnetic (NM) phase to the ferromagnetic (FM) phase with increasing temperature. Using the canonical partition function in terms of three magnetic microstates of the grand FM state and the metastable NM and antiferromagnetic (AFM) states<sup>[21, 24]</sup>, the predicted miscibility gap and isobaric volumes at five pressures are plotted in Figure 6 as a function of temperature. Available experimental data are also included, agreeing well with the predictions, see details in [14]. Figure 6 shows that fcc Ce belongs to a single-phase region at all temperatures considered in the pressure range of 2.25 ~ 3.5 GPa. In this pressure range, normal thermal expansion is expected at both the low and high temperatures on each isobaric curve<sup>[14]</sup>. However in the middle temperature range on each isobaric curve (highlighted by the open diamond symbols), CPTE exists due to the fast increase of thermal probability of the metastable microstates with respect to temperature, see especially the curve with the pressure of 2.25 GPa, representing the critical point.

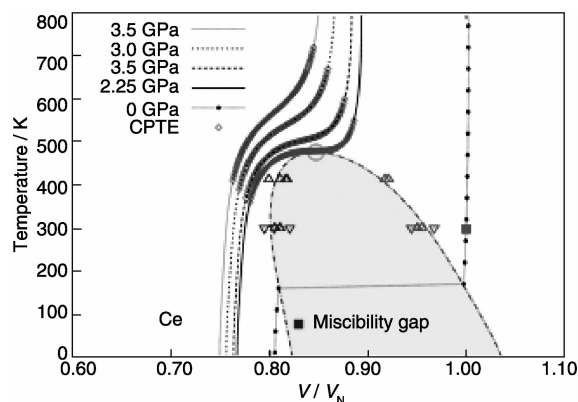


Fig. 6 Isobaric volumes of fcc Ce at five pressures. The volume ( $V$ ) is normalized to its equilibrium volume ( $V_N$ ) at stand pressure and temperature. The predicted CPTE regions are shown by the gray open diamonds, and the light gray open circle indicates the critical point. Details of first-principles methodology and references for experimental data (symbols except for the gray open diamonds) are given in the literature [14, 21, 24]

For disordered phase containing two and more microstates, the examples of CZTS, fcc Ce, and the aforementioned ones indicate that the (grand) canonical partition function can be used to quantitatively tailor disordered phase and associated anomalous properties. In practice, the ensemble can be selected based on crystallographic unit cell or its supercell, and all microstates within this ensemble should be accounted for in order to satisfy the condition of ergodicity in statistical physics. For example of a binary bcc phase, a  $2 \times 2 \times 2$  supercell with 16 atomic sites possesses  $2^{16} = 65,536$  microstates, but only 331 of them are independent. These independent microstates and the associated degeneracy factors can be generated using e. g. the *genstr* code (updated by the present author YW) within the ATAT package<sup>[60]</sup>. In principle, the larger the supercell/ensemble,

the more accurate the results will be obtained. The amount of microstates around thousand is within the current capability of first-principle calculations. Based on our studies of CZTS<sup>[10]</sup>, bcc Fe<sup>[19]</sup>, and fcc Ni<sup>[25]</sup>, fcc Ce<sup>[21, 24]</sup>, Fe<sub>3</sub>Pt<sup>[20]</sup>, and Be-Fe<sub>2</sub>As<sub>2</sub><sup>[22]</sup>, a supercell/ensemble with 16 or less atomic sites for disordered atoms, resulting in hundreds or less independent microstates for binary system, is big enough to study the properties of interest. In addition, an integrated first-principles, CEM, and partition function approach can be applied to study an ensemble using larger supercells. Note also that only the macroscopically homogeneous single phase for a given material is the present focus since the partition function approach is faced to phase consisting of microstates.

## 4 Summary

The present work provide a perspective on the macroscopically homogeneous single “phase”, which can be depicted as a statistical ensemble consisting of one primary microstate (i. e., the ordered phase) or more noticeable microstates (i. e., the disordered phase). A DFT-based canonical (or grand canonical) partition function in terms of microstates is emerging as a key approach to describe disordered phase and associated anomalous properties. For a given microstate, the quasiharmonic approach in terms of first-principles phonon calculations is able to predict its thermodynamic properties. In addition, a quasistatic approach can be used to depict properties of interest at finite temperatures, such as elasticity, stacking fault, and ideal strength. It is shown that (i) the description of a macroscopically homogeneous “phase” in terms of “microstate(s)” opens a new pathway to quantitatively tailor anomalous properties such as thermal expansion and heat capacity, which are traceable from the microstate configurational entropy, and (ii) these microstates can be considered as the building blocks, i. e., the genome, of materials. Examples in the present work are given for the ordered phases of anti-fluorite Li<sub>2</sub>S, hcp Mg, and fcc Ni as well as the disordered phases of Cu<sub>2</sub>ZnSnS<sub>4</sub> (CZTS) and fcc Ce in order to demonstrate the current advance of first-principles thermodynamics at finite temperatures.

**Acknowledgements** This work was financially supported by the U. S. national science foundation (NSF) with Grant Nos. DMR-1006557, CHE-1230929, DMR-1310289, and CMMI-1333999. First-principles calculations were carried out partially on the LION clusters at the Pennsylvania State University, partially on the resources of NERSC supported by the Office of Science of the U. S. Department of Energy under contract No. DE-AC02-05CH11231, and partially on the resources of XSEDE supported by NSF with Grant No. ACI-1053575.

## References

- [1] Liu Z K. First-Principles Calculations and CALPHAD Modeling of Thermodynamics [J]. *J Phase Equilib Diff*, 2009, 30: 517–534.

- [2] Shang S L, Wang Y, Kim D, *et al.* First-Principles Thermodynamics from Phonon and Debye Model: Application to Ni and Ni<sub>3</sub>Al [J]. *Comput Mater Sci*, 2010, 47: 1 040 – 1 048.
- [3] Wang Y, Liu Z K, Chen L Q. Thermodynamic Properties of Al, Ni, NiAl, and Ni<sub>3</sub>Al from First-Principles Calculations [J]. *Acta Mater*, 2004, 52: 2 665 – 2 671.
- [4] Shang S L, Wang Y, Kim D E, *et al.* Structural, Vibrational, and Thermodynamic Properties of Ordered and Disordered Ni<sub>1-x</sub>Pt<sub>x</sub> Alloys from First-Principles Calculations [J]. *Phys Rev B*, 2011, 83: 144 204.
- [5] Connolly J W D, Williams A R. Density-Functional Theory Applied to Phase Transformations in Transition-Metal alloys [J]. *Phys Rev B*, 1983, 27: 5 169 – 5 172.
- [6] Van de Walle A, Ceder G. Automating First-Principles Phase Diagram Calculations [J]. *J Phase Equilib*, 2002, 23: 348 – 359.
- [7] Van De Walle A. A Complete Representation of Structure-Property Relationships in Crystals [J]. *Nature Mater*, 2008, 7: 455 – 458.
- [8] Zunger A, Wei S H, Ferreira L G, *et al.* Special Quasirandom Structures [J]. *Phys Rev Lett*, 1990, 65: 353 – 356.
- [9] Jiang C, Wolverton C, Sofo J, *et al.* First-Principles Study of Binary bcc Alloys Using Special Quasirandom Structures [J]. *Phys Rev B*, 2004, 69: 214202.
- [10] Shang S L, Wang Y, Lindwall G, *et al.* Cation Disorder Regulation by Microstate Configurational Entropy in Photovoltaic Absorber Materials Cu<sub>2</sub>ZnSn(S, Se)<sub>4</sub> [J]. *J Phys Chem C*, 2014, 118: 24 884 – 24 889.
- [11] Shang S, Wang Y, Wang W Y, *et al.* Low Energy Structures of Lithium-Ion Battery Materials Li(Mn<sub>x</sub>Ni<sub>x</sub>Co<sub>1-2x</sub>)O<sub>2</sub> Revealed by First-Principles Calculations [J]. *Appl Phys Lett*, 2013, 103: 053 903.
- [12] Shang S L, Wang Y, Du Y, *et al.* Entropy Favored Ordering: Phase Stability of Ni<sub>3</sub>Pt Revisited by First-Principles [J]. *Intermetallics*, 2010, 18: 961 – 964.
- [13] Shang S, Bottger A. A Combined Cluster Variation Method and Ab Initio Approach to the Gamma-Fe[N]/Gamma'-Fe<sub>4</sub>N<sub>1-x</sub> Phase Equilibrium [J]. *Acta Mater*, 2005, 53: 255 – 264.
- [14] Liu Z K, Wang Y, Shang S. Thermal Expansion Anomaly Regulated by Entropy [J]. *Sci Rep*, 2014, 4: 7 043.
- [15] Garrod C. *Statistical Mechanics and Thermodynamics* [M]. New York: Oxford University Press, 1995.
- [16] Liu Z K. Perspective on Materials Genome® [J]. *Chinese Science Bulletin*, 2014, 59: 1 619 – 1 623.
- [17] Wang Y, Wang J J, Wang W Y, *et al.* A Mixed-Space Approach to First-Principles Calculations of Phonon Frequencies for Polar Materials [J]. *J Phys-Condens Matter*, 2010, 22: 202 201.
- [18] Wang Y, Chen L Q, Liu Z K. YPHON: A Package for Calculating Phonons of Polar Materials [J]. *Comput Phys Commun*, 2014, 185: 2 950 – 2 968.
- [19] Shang S L, Wang Y, Liu Z K. Thermodynamic Fluctuations Between Magnetic States from First-Principles Phonon Calculations: The Case of bcc Fe [J]. *Phys Rev B*, 2010, 82: 014 425.
- [20] Wang Y, Shang S L, Zhang H, *et al.* Thermodynamic Fluctuations in Magnetic States: Fe<sub>3</sub>Pt as a Prototype [J]. *Philos Mag Lett*, 2010, 90: 851 – 859.
- [21] Wang Y, Hector L G, Zhang H, *et al.* A Thermodynamic Framework for a System with Itinerant – Electron Magnetism [J]. *J Phys-Condens Matter*, 2009, 21: 326 003.
- [22] Wang Y, Shang S L, Chen L Q, *et al.* Magnetic Excitation and Thermodynamics of BaFe<sub>2</sub>As<sub>2</sub> [J]. *Inter J Quan Chem*, 2011, 111: 3 565 – 3 570.
- [23] Sadus R J. *Molecular Simulation of Fluids: Theory, Algorithms and Object-orientation* [M]. Amsterdam: Elsevier, 1999.
- [24] Wang Y, Hector L G, Zhang H, *et al.* Thermodynamics of the Ce Gamma-Alpha Transition: Density-Functional Study [J]. *Phys Rev B*, 2008, 78: 104 113.
- [25] Shang S L, Saal J E, Mei Z G, *et al.* Magnetic Thermodynamics of fcc Ni from First-Principles Partition Function Approach [J]. *J Appl Phys*, 2010, 108: 123 514.
- [26] Shang S L, Wang Y, Mei Z G, *et al.* Lattice Dynamics, Thermodynamics, and Bonding Strength of Lithium-Ion Battery Materials LiMPO<sub>4</sub> (M = Mn, Fe, Co, and Ni): A Comparative First-Principles Study [J]. *J Mater Chem*, 2012, 22: 1 142 – 1 149.
- [27] Shang S L, Hector L G, Shi S Q, *et al.* Lattice Dynamics, Thermodynamics and Elastic Properties of Monoclinic Li<sub>2</sub>CO<sub>3</sub> from Density Functional Theory [J]. *Acta Mater*, 2012, 60: 5 204 – 5 216.
- [28] Mei Z G, Wang Y, Shang S L, *et al.* First-Principles Study of Lattice Dynamics and Thermodynamics of TiO<sub>2</sub> Polymorphs [J]. *Inorg Chem*, 2011, 50: 6 996 – 7 003.
- [29] Wang Y, Fang H, Zacherl C L, *et al.* First-Principles Lattice Dynamics, Thermodynamics, and Elasticity of Cr<sub>2</sub>O<sub>3</sub> [J]. *Surf Sci*, 2012, 606: 1 422 – 1 425.
- [30] Wang Y, Saal J E, Wang J J, *et al.* Broken Symmetry, Strong Correlation, and Splitting between Longitudinal and Transverse Optical Phonons of MnO and NiO from First Principles [J]. *Phys Rev B*, 2010, 82: 081 104.
- [31] Wang Y, Saal J E, Mei Z G, *et al.* A First-Principles Scheme to Phonons of High Temperature Phase: No Imaginary Modes for Cubic SrTiO<sub>3</sub> [J]. *Appl Phys Lett*, 2010, 97: 162 907.
- [32] Wang Y, Saal J E, Wu P P, *et al.* First-Principles Lattice Dynamics and Heat Capacity of BiFeO<sub>3</sub> [J]. *Acta Mater*, 2011, 59: 4 229 – 4 234.
- [33] Wang Y, Wang J J, Saal J E, *et al.* Phonon Dispersion in Sr<sub>2</sub>RuO<sub>4</sub> Studied by a First-Principles Cumulative Force-Constant Approach [J]. *Phys Rev B*, 2010, 82: 172 503.
- [34] Wang Y, Zhang L A, Shang S, *et al.* Accurate Calculations of Phonon Dispersion in CaF<sub>2</sub> and CeO<sub>2</sub> [J]. *Phys Rev B*, 2013, 88: 024 304.
- [35] Shang S L, Zhang H, Wang Y, *et al.* Temperature-Dependent Elastic Stiffness Constants of Alpha- and Theta-Al<sub>2</sub>O<sub>3</sub> from First-Principles Calculations [J]. *J Phys-Condens Matter*, 2010, 22: 375 403.
- [36] Wang Y, Wang J J, Zhang H, *et al.* A First-Principles Approach to Finite Temperature Elastic Constants [J]. *J Phys-Condens Matter*, 2010, 22: 225 404.
- [37] Zhang H, Shang S L, Wang Y, *et al.* First-Principles Calculations of the Elastic, Phonon and Thermodynamic Properties of Al<sub>12</sub>Mg<sub>17</sub> [J]. *Acta Mater*, 2010, 58: 4 012 – 4 018.
- [38] Ganeshan S, Shang S L, Wang Y, *et al.* Temperature Dependent

- Elastic Coefficients of  $\text{Mg}_2X$  ( $X = \text{Si}, \text{Ge}, \text{Sn}, \text{Pb}$ ) Compounds from First-Principles Calculations [J]. *J Alloys Compd*, 2010, 498: 191–198.
- [39] Wrobel J, Hector L G, Wolf W, *et al.* Thermodynamic and Mechanical Properties of Lanthanum-Magnesium Phases from Density Functional Theory [J]. *J Alloys Compd*, 2012, 512: 296–310.
- [40] Shang S L, Kim D E, Zacherl C L, *et al.* Effects of Alloying Elements and Temperature on the Elastic Properties of Dilute Ni-Base Superalloys from First-Principles Calculations [J]. *J Appl Phys*, 2012, 112: 053 515.
- [41] Wang A, Shang S L, He M, *et al.* Temperature-Dependent Elastic Stiffness Constants of fcc-Based Metal Nitrides from First-Principles Calculations [J]. *Journal of Materials Science*, 2014, 49: 424–432.
- [42] Dri F L, Shang S L, Hector L G, *et al.* Anisotropy and Temperature Dependence of Structural, Thermodynamic, and Elastic Properties of Crystalline Cellulose I-Beta; a First-Principles Investigation [J]. *Modelling Simul Mater Sci Eng*, 2014, 22: 085 012.
- [43] Shang S L, Wang W Y, Wang Y, *et al.* Temperature-Dependent Ideal Strength and Stacking Fault Energy of fcc Ni; A First-Principles Study of Shear Deformation [J]. *J Phys-Condens Matter*, 2012, 24: 155 402.
- [44] Kresse G, Furthmuller J. Efficient Iterative Schemes for Ab Initio Total-Energy Calculations Using a Plane-Wave Basis Set [J]. *Phys Rev B*, 1996, 54: 11 169–11 186.
- [45] Kresse G, Joubert D. From Ultrasoft Pseudopotentials to the Projector Augmented-Wave Method [J]. *Phys Rev B*, 1999, 59: 1 758–1 775.
- [46] Shang S L, Wang Y, Guan P W, *et al.* Insight into Structural, Elastic, Phonon, and Thermodynamic Properties of  $\alpha$ -Sulfur and Energy-Related Sulfides; A Comprehensive First-Principles Study [J]. *J Mater Chem A*, 2015, 3: 8 002–8 014.
- [47] Perdew J P, Burke K, Ernzerhof M. Generalized Gradient Approximation Made Simple [J]. *Phys Rev Lett*, 1996, 77: 3 865–3 868.
- [48] Perdew J P, Ruzsinszky A, Csonka G I, *et al.* Restoring the Density-Gradient Expansion for Exchange in Solids and Surfaces [J]. *Phys Rev Lett*, 2008, 100: 136 406.
- [49] Grimme S, Antony J, Ehrlich S, *et al.* A Consistent and Accurate Ab Initio Parametrization of Density Functional Dispersion Correction (DFT-D) for the 94 Elements H-Pu [J]. *J Chem Phys*, 2010, 132: 154 104.
- [50] Heyd J, Scuseria G E, Ernzerhof M. Hybrid Functionals Based on a Screened Coulomb Potential [J]. *J Chem Phys*, 2003, 118: 8 207–8 215.
- [51] Blöchl P E, Jepsen O, Andersen O K. Improved Tetrahedron Method for Brillouin-Zone Integrations [J]. *Phys Rev B*, 1994, 49: 16 223–16 233.
- [52] Scientific Group Thermodata Europe (SGTE), ed. *Thermodynamic Properties of Inorganic Materials*[M]. Berlin: Springer, 1999.
- [53] Buehrer W, Altorfer F, Mesot J, *et al.* Lattice-Dynamics and the Diffuse Phase-Transition of Lithium Sulfide Investigated by Coherent Neutron-Scattering [J]. *J Phys-Condens Matter*, 1991, 3: 1 055–1 064.
- [54] Grzechnik A, Vegas A, Syassen K, *et al.* Reversible Antifluorite to Anticotunnite Phase Transition in  $\text{Li}_2\text{S}$  at High Pressures [J]. *J Solid State Chem*, 2000, 154: 603–611.
- [55] Bertheville B, Bill H, Hagemann H. Experimental Raman Scattering Investigation of Phonon Anharmonicity Effects in  $\text{Li}_2\text{S}$  [J]. *J Phys Condens Matter*, 1998, 10: 2 155–2 169.
- [56] Khachai H, Khenata R, Bouhemadou A, *et al.* FP-APW + LO Calculations of the Electronic and Optical Properties of Alkali Metal Sulfides under Pressure [J]. *J Phys-Condens Matter*, 2009, 21: 095 404.
- [57] Shang S L, Liu Z K. *Thermodynamic Properties of Magnesium Alloys*, in *Fundamentals of Magnesium Alloy Metallurgy*[M]. Cambridge: Woodhead Publishing, 2013, 85–124.
- [58] Scragg J J S, Choubac L, Lafond A, *et al.* A Low-Temperature Order-Disorder Transition in  $\text{Cu}_2\text{ZnSnS}_4$  Thin Films [J]. *Appl Phys Lett*, 2014, 104: 041 911.
- [59] Schorr S, Gonzalez-Aviles G. In-Situ Investigation of the Structural Phase Transition in Kesterite [J]. *Phys Status Solidi A*, 2009, 206: 1 054–1 058.
- [60] Van De Walle A, Tiwary P, De Jong M, *et al.* Efficient Stochastic Generation of Special Quasirandom Structures [J]. *Calphad*, 2013, 42: 13–18.

(编辑 盖少飞 惠 琼)